Materials Advances

ROYAL SOCIETY OF CHEMISTRY

PAPER

View Article Online
View Journal | View Issue

Open Access Article. Published on 03 January 2025. Downloaded on 10/26/2025 6:04:59 AM.
This article is licensed under a Creative Commons Attribution-NonCommercial 3.0 Unported Licence.

Check for updates

Cite this: *Mater. Adv.*, 2025, **6**, 1288

Gum arabic-CNT reinforced hydrogels: dual-function materials for strain sensing and energy storage in next-generation supercapacitors

Tanzil UrRehman,[a] Sher Ali Khan,[a] Luqman Ali Shah *[a] and Jun Fu [b]

Received 2nd October 2024,
Accepted 26th December 2024

DOI: 10.1039/d4ma00992d

rsc.li/materials-advances

Recent advancements in the field of conductive hydrogels have made the hydrogels promising candidates for the development of human motion sensors, as well as for energy storage in soft and flexible electronic devices, owing to their excellent mechanical properties such as flexibility, bioavailability, and biocompatibility. However, limitations such as resilience, resistance to fatigue, toughness, flexibility, and stretchability have hampered their sensing capabilities and long-term operation. To address these limitations, we introduced an ionically and electronically conductive hydrogel composite, which is aimed at enhancing mechanical performance and responsiveness to human motion, ranging from finger bending to epidermal motion sensing. This hydrogel was synthesized by incorporating an unmodified electroactive material, carbon nanotubes (CNTs), stabilized by the biopolymer gum arabic (GA) within the hydrophobically associated hydrogels of lauryl methacrylate (LM) and polyacrylamide (p(Am)). The dispersion of both LM and CNTs was facilitated by the anionic surfactant sodium dodecyl sulfate (SDS). The introduction of CNTs and varying the concentration of GA highly enhanced the mechanical property of the synthesized hydrogel, which in turn brilliantly improved its stretchability up to 1380%, with an antifatigue character and a toughness of 661.5 kJ m^{-3}. The high tensile strain sensitivity of the hydrogel material, with a gauge factor (GF) of 9.45 at 1000% strain, demonstrated its remarkable sensitivity. The composite hydrogels exhibited impressive sensing capabilities, including differentiation in language, response to high and low pitches and stresses, drawing various shapes, writing different words, and detection of various human actions. The critical strain study of the present materials underscored their excellent rheological properties. The hydrogels with CNT addition and higher concentrations of GA demonstrated specific capacitance (Cs) values of 171.25 F g^{-1} from CV at 20 mV s^{-1}, 113.7 F g^{-1} from GCD at a current density of 0.3 A g^{-1}, and a resistance of 7.656 Ω measured *via* EIS at a frequency of 5 mV. These electrochemical properties highlight the potential use of hydrogels for energy storage in soft wearable electronic devices.

1. Introduction

Soft wearable electronic sensors with stretchable and flexible strain have attracted much[1] research attention owing to their versatile potential application and use[2] in many fields such as human motion sensing,[3,4] epidermal stretching sensing,[5,6] health-related monitoring,[7] energy harvesting[8] and storage. The main applications of these soft robotic devices include the detection of biological activities[9,10] and mechanical action *via* electrical and conductivity changes during routine operation.[11,12] For decades, researchers have strived to enhance the mechanical properties and conductivity of polymeric materials through fillers and electroactive materials such as bioavailable[13] and synthetic polymers as well as using electroactive carbon-based materials such as graphene, graphene oxide (GO), reduced graphene oxide (rGO), reduced magnetite graphene oxide (rMGO), carbon nanotubes (CNTs)[14–18] and even polymers that are conductive in nature. Nevertheless, soft flexible wearable electronic robotic devices have many limitations in terms of their endurance, extended sensing response times, weak mechanical performance, predisposition to electrical conduction, and loss of electrical transmission and conductivity upon high deformation.[17] Because of these challenges, the manufacturing of such flexible hydrogels has been limited toward potential application. Thus, it is necessary to develop

[a] *Polymer Laboratory, National Centre of Excellence in Physical Chemistry, University of Peshawar, 25120, Pakistan. E-mail: luqman_alisha@uop.edu.pk, Luqman_alisha@yahoo.com; Fax: +92-91-9216671; Tel: +92-91-9216766*
[b] *Key Laboratory of Polymeric Composite and Functional Materials, School of Materials Science and Engineering, Sun Yat-sen University, Guangzhou 510275, China*

© 2025 The Author(s). Published by the Royal Society of Chemistry

Open Access Article. Published on 03 January 2025. Downloaded on 10/26/2025 6:04:59 AM.
This article is licensed under a Creative Commons Attribution-NonCommercial 3.0 Unported Licence.

and enhance the flexible, conductive, and stretchable properties of hydrogels that can retain their stretchability and conductivity even after different and long ranges of strain. Such progress and advancement of novel stretchable and flexible conductive hydrogels reduce the challenges and problems faced by the materials reported earlier in the literature.[19,20]

In this aspect, hydrogels that can uptake water and soft materials provide the opportunity to develop soft wearable electronic sensors, along with their bioavailability, biocompatibility, biodegradability, and conductivity. In this regard, one can approach the development of such hydrogel materials (which are effective regarding their application) *via* chemical and physical cross linking, using fillers for enhancing the mechanical properties, organic and inorganic composites, and electroactive materials. Besides this, one can create the hydrogel with a double network (DN),[21] interpenetrating network (IPN),[22] and semi-IPN for its potential uses.[23] For such uses, the polymeric hydrogel material must possess excellent mechanical performance with respect to the tensile strength,[24] toughness and novel recoverability to face long-range deformability after applied forces.[25,26] The material also will be more effective if it can sense conductivity for high-range deformation, as well as the large number of cyclic stabilities during its routine operation. Thus, researchers in the field (especially in the advancement of applied materials) have focused their efforts to develop hydrogels with enhanced toughness, tensile strength, conductivity, and self-shape recovery[27] by introducing and developing mechanical bonds (non-covalent) like H-bonding, ionic, and hydrophobic association within the hydrogel network.[28,29]

To enhance the self-recovery, hydrophobic association (HA) and ionic association might be better suited for the material candidates.[30] HA depends mostly on monomers that are intrinsically hydrophobic due to the presence of the water-repellent alkyl group (–CH_3–CH_2–), and makes the molecule stretchable with respect to applied stress and managing the energy dissipation.[28] Surfactants are used for the homogenous distributions of hydrophobic monomers to stabilize the hydrophobic association *via* micelles.[31] The distribution of hydrophobic monomers, along with hydrophilic monomers within the network, thus enhances the interaction within the entire network. For mechanical character enhancement, chemical crosslinking is typically selected. However, such covalently bonded materials are irreversible and show poor recovery, and are thus weak to resist fatigue.[32] To overcome this issue, hydrophobic physical crosslinking was introduced by researchers to achieve resilience, stretchability, and self-recovery at high stress upon longer deformation. Similarly, researchers also used carbon-based materials to enhance the conductivity and mechanical properties.

In the current study, a one-pot method was employed to synthesize a hydrophobically associated polymeric hydrogel using the hydrophobic monomer lauryl methacrylate (LM). This monomer stabilizes SDS micelles, and SDS reciprocally stabilizes LM. Upon polymerization, LM was polymerized with its hydrophilic end interacting with polymeric acrylamide p(Am) and a biopolymer, thereby physically cross-linking the entire hydrogel network matrix. The incorporation of electroactive materials like CNTs and NaCl resulted in a conductive hydrogel, which is potentially useful for long-range human motion sensing. Additionally, biopolymers such as gum arabic (GA) served as stabilizers for unmodified CNTs and fillers to enhance mechanical properties, owing to their abundant –OH group functionalities that facilitate hydrogen bonding. Hydrogels with fillers and electroactive materials present promising candidates for human motion detection and strain sensing due to their high cyclic stability, excellent conductivity, favorable elastic behavior, low energy hysteresis, and applicability in soft electronic energy storage devices like supercapacitors. The synthesized material exhibited sensitivity to strains ranging from 50% to 900%, and a response time of 0.29 s with good cyclic stability. Furthermore, the synthesized materials demonstrated successful responses to various gestures when connected to different parts of the human body, including fingers, elbows, knee joints, and vocal cords, enabling the detection of different words and alphabets.

2. Materials and synthesis

2.1. Materials

The following analytical grade chemicals were used as received during the present experimental work: acrylamide (AAm, Sigma Aldrich), gum arabic (GA, Sigma Aldrich), lauryl methacrylate (LM, Agros), sodium dodecyl sulphate (SDS, BDH), multiwall carbon nanotubes (MWCNTs), sodium chloride (NaCl, BDH), and ammonium persulphate (APS). Purified distilled water was used throughout all experimental procedures.

2.2. Synthesis of hydrophobically associated hydrogels

The synthesis of hydrophobically associated polymeric hydrogels was achieved *via* free radical polymerization. First, 0.4 g of SDS and 0.25 g of NaCl were stirred in 8 mL of water. Subsequently, 300 μL of lauryl methacrylate (LM) was added to the surfactant solution. Then, 2 g of AAm was added, followed by the addition of GA as a filler with different percentages (0.02 g (1%), 0.03 g (2%), and 0.04 g (3%)) with respect to the amount of AAm (2 g). APS (0.05 g) was used as a thermal initiator. CNTs (0.001 g) was homogenized with GA and SDS in separate beakers to make stable colloids. The solution was slowly and gradually added to the AAm mixture. All the mixtures were then poured into the plastic molds, and kept in the oven for 30 min at 60 °C. After successful preparation, the hydrogels were washed and stored for further applications. The samples were labeled as G1-CNT_0, G1-CNT, G2-CNT, and G3-CNT according to the percentage of GA (1% to 3%).

2.3. Hydrogels characterization

The materials were freeze-dried for 24 hours prior to the different characterizations. For the determination of the interaction and functionalities within the hydrogel network materials, a Fourier transform infrared spectrophotometer (FT-IR) (Anton Paar Germany) was used. For characterizing the surface texture

Open Access Article. Published on 03 January 2025. Downloaded on 10/26/2025 6:04:59 AM.
This article is licensed under a Creative Commons Attribution-NonCommercial 3.0 Unported Licence.

and morphology, a scanning electron microscope (Jeol Japan) was operated at 15 kV voltage. A universal testing machine (UTM) with a 30 kN load cell and speed of 50 mm min^{-1} was used to check the tensile strength, loading and unloading, and multiple cycles to determine the mechanical properties of the synthesized samples. The area under the stress–strain curves was determined to elucidate the toughness of the hydrogels and energy dissipation during the loading and un-loading process.[33]

The rheological characteristics of the produced hydrogels were assessed using an Anton Paar (MCR 301) rheometer equipped with a 25 mm rotating disc attachment. Cubic samples of the hydrogel, measuring 18 mm in width and length with a thickness of 3 mm, were prepared for testing. Both frequency and amplitude sweep tests were conducted at a constant temperature of 25 °C. The frequency sweep ranged from 0 to 100 rad s^{-1}, while the strain range for hydrogel analysis was set from 0.01% to 1000%.

2.4. Strain sensitivity and electrochemical analysis

To evaluate conductivity, the samples were subjected to electrical measurements using specialized instrumentation. A Metrhom Auto Lab workstation (Netherlands) was used to assess the conductivity, strain sensitivity, and the electrochemical response of the hydrogel materials. A two-electrode system was employed for conductivity and strain sensitivity analyses, while a three-electrode electrochemical work station assembly was utilized for investigating the electrochemical responses, including cyclic voltammetry (CV), galvanostatic charge–discharge (GCD), and electrochemical impedance spectroscopy (EIS). The conductivity (measured in Siemens per meter, 0.142 S m^{-1}) was calculated using eqn (1):

$$\sigma = \frac{L \cdot 100}{R_s A} \quad (1)$$

where σ represents the conductivity (S m^{-1}), R_s denotes the resistance (Ω) of the substance in bulk, A signifies the electrode and hydrogel surface area, and L (cm) represents the distance between them. To observe the conductivity and strain sensing of the synthesized hydrogels, LED (4.2 V) illumination bulbs were employed for direct observation of the hydrogel response to stretching and bending, allowing for monitoring the illumination response. However, precise strain sensing tests were conducted by connecting the hydrogel material to a two-electrode probe and tested using chronoamperometry (current (I) *versus* time (T)). The hydrogel samples were cut to specific dimensions, and then attached to the human epidermis for the detection of various human motions.

3. Results and discussion

The hydrogels were successfully characterized using FTIR and SEM analysis. The FTIR spectra of G1-CNT_0 and G3-CNT are shown in Fig. 1a. The 3334 cm^{-1} stretching peak of –OH from the polysaccharide GA structure is reduced in the CNT-reinforced hydrogel, which is attributed to the interaction *via* hydrogen bonding of the $^{-}$OH group with the polymeric network, as well as an increase in the number of hydroxyl groups.[34] The CNT incorporation also reduced the free vibration of the $^{-}$OH group. Similarly, the reduced intensity of the peaks at 2944 and 2923 cm^{-1} (–C–H stretching vibration) is probably attributable to van der Waals association within the gel matrix.[35] The appearance of a shoulder peak at 1730 cm^{-1} shows the stretching vibration of carboxylic group (–C═O), which indicated the successive incorporation of CNTs within the hydrogel network.[36,37] A peak at 1657 cm^{-1} (–C═O) in both samples and its reduction intensity in G3-CNT is probably attributed to the involvement of the group in the association.[38] Similarly, the peak with the intensity reduction at 1465 cm^{-1} is assigned to the –OH bending vibration, which is present in both samples. There is an increase in the intensity of the peak at 1260 cm^{-1} in the case of G3-CNT, which is probably the C–C skeletal vibration, and shows the homogenization of CNTs inside the matrix. Reduction of the peak at 1213 cm^{-1} also supports the ceasing of the –C–H skeletal vibration, showing the hydrophobic association of CNT with hydrophobic microregions created within the hydrogel network. The disappearance of a small peak at 723 cm^{-1} in sample G3-CNT (–C–H out-of-plane vibration) supports the hydrophobic interaction of CNT with the polymeric chain of the synthesized hydrogel. The peak at 1019 cm^{-1} shows –C–O–C bending vibration, and intensity reduction is reflective of G3-CNT involvement in H-bond formation in the polymeric chain of the hydrogel network.[39] The possible interactions and associations that created a change and enhanced the properties of the hydrogel with the addition of CNT are indicated in Fig. 1b.

The surface texture and morphology of the synthesized hydrogels were examined *via* SEM, as shown in Fig. 1(c–f). The hydrogel composed of GA, LM, and AAm having physical and hydrophobic association without CNT shows a less porous surface, which hinders the mobility of ions (Fig. 1c). However, it can be observed from Fig. 1d that a more porous structure is developed by increasing the percentage of GA and adding CNT. Furthermore, increasing the GA percentage enables uniform porosity distribution within the hydrogel matrix, probably due to the complete dispersion of CNT and its stabilization by GA in the synthesized hydrogels (Fig. 1e and f). Such uniform porosity and stabilization of CNT in the network make the hydrogels porous, and provide an appropriate medium for ion and electron transport, making them conductive.

3.1. Mechanical performance

The tensile test was performed to characterize the effect of the reinforcer CNT and GA concentration on the stretchability of the hydrophobically associated hydrogels (Fig. 2). The results indicate that the stretchability increases with increasing reinforcer content within the hydrogel matrix. It can be noted from Fig. 2a that in the absence of CNT and with a low amount of GA in the hydrogel (G1-CNT_0), the stretchability is 530% with a stress value of 352 kPa, while the stretchability reached up to 956% with a stress value of 1241 kPa for G3-CNT having a higher concentration of GA. Another finding is the enhancement in the fracture strain, which is 25% for G1-CNT_0. However, the fracture strain increases up to 48% after the addition of CNT at 439 kPa of fracture stress. Keeping the CNT concentration constant, the amount of GA was increased in the hydrogel matrix with

 © 2025 The Author(s). Published by the Royal Society of Chemistry

Open Access Article. Published on 03 January 2025. Downloaded on 10/26/2025 6:04:59 AM.
This article is licensed under a Creative Commons Attribution-NonCommercial 3.0 Unported Licence.

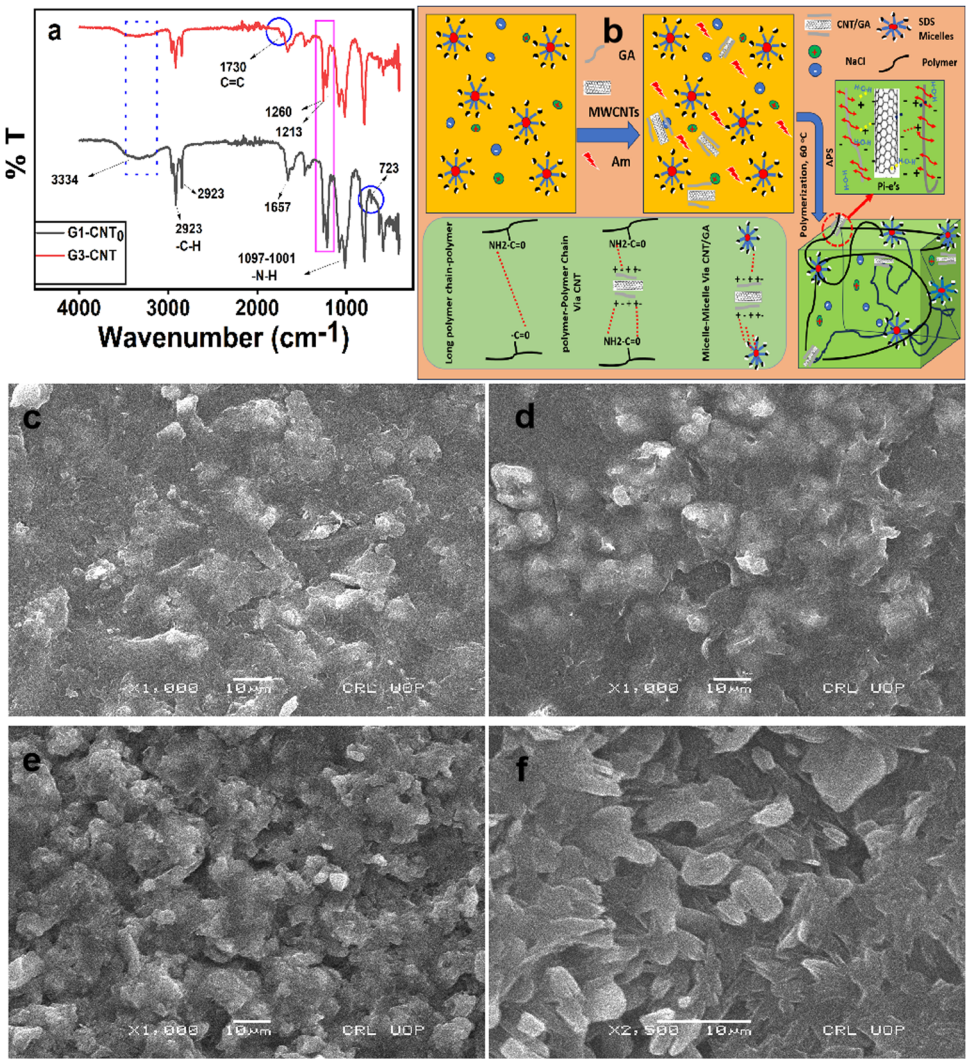

Fig. 1 (a) FT-IR spectra, (b) the existence of a possible interaction in the hydrogel network, and SEM images of (c) G1-CNT$_0$, (d) G1-CNT, (e) G2-CNT, and (f) G3-CNT.

respect to AAm. It was observed that the fracture strain increased to 1274% (661 kPa) in 3% of GA, but the fracture strain decreased to 1216% at 1241 kPa of stress for the sample containing 4% of GA (Fig. 2b). This behavior of the as-synthesized hydrogel suggests the existence of hydrophobic association and hydrogen bonding. The H-bonding is due to the increase in the GA concentration, which accumulates a larger number of hydroxyl groups in the polymeric chain, resulting in the bulk (dense) crosslinking in the hydrogel network and making the material mechanically better. This also confirms the positive effect of GA addition in enhancing the mechanical behavior of the mechanically weak hydrogel and polymeric materials. Such development of dynamic and non-covalent bonds contribute to the stretchability, with the higher strain and stress fracture value making the materials more valuable and workable. It was further observed that such non-covalent higher crosslinking with increased GA concentration not only boosts the fracture stress and strain, but also changes the other parameters such as stiffness (Young modulus) and fracture energy (toughness) of the as-synthesized hydrogels. From Fig. 2c, it can be interpreted that both fracture energy and Young modulus increases. The fracture energy increases from 100 to 650 kJ m^{-3} for sample G1-CNT$_0$ to G3-CNT, respectively. Furthermore, the Young modulus values for samples G1-CNT$_0$, G1-CNT, G2-CNT, and G3-CNT were 1.19, 1.2, 3.19, and 4.211 kPa, respectively, indicating the enhancement in the Young modulus with increasing GA addition as a reinforcing agent to achieve better performance of the materials in human motion and flexible electronic devices.

Similarly, the non-covalent and mechanical properties of the synthesized hydrogel (G3-CNT due to its better tensile characteristics) were further characterized *via* cyclic tensile test by keeping the hydrogel in a testometer under cyclic loading-unloading for five times at 800% strain and ordinary room temperature without any time interval (Fig. 2d). A slight dissipation takes place in the first cycle, followed by a negligible decrease in the dissipated energy from the second to fifth cycle. This study shows the stability of the hydrogels to be used as strain sensors in different devices.

It was found that the dissipation energy wasted in the 1st cycle was 23.06 kJ m^{-3} at 250 kPa of stress. The lower energy at

Open Access Article. Published on 03 January 2025. Downloaded on 10/26/2025 6:04:59 AM.
This article is licensed under a Creative Commons Attribution-NonCommercial 3.0 Unported Licence.

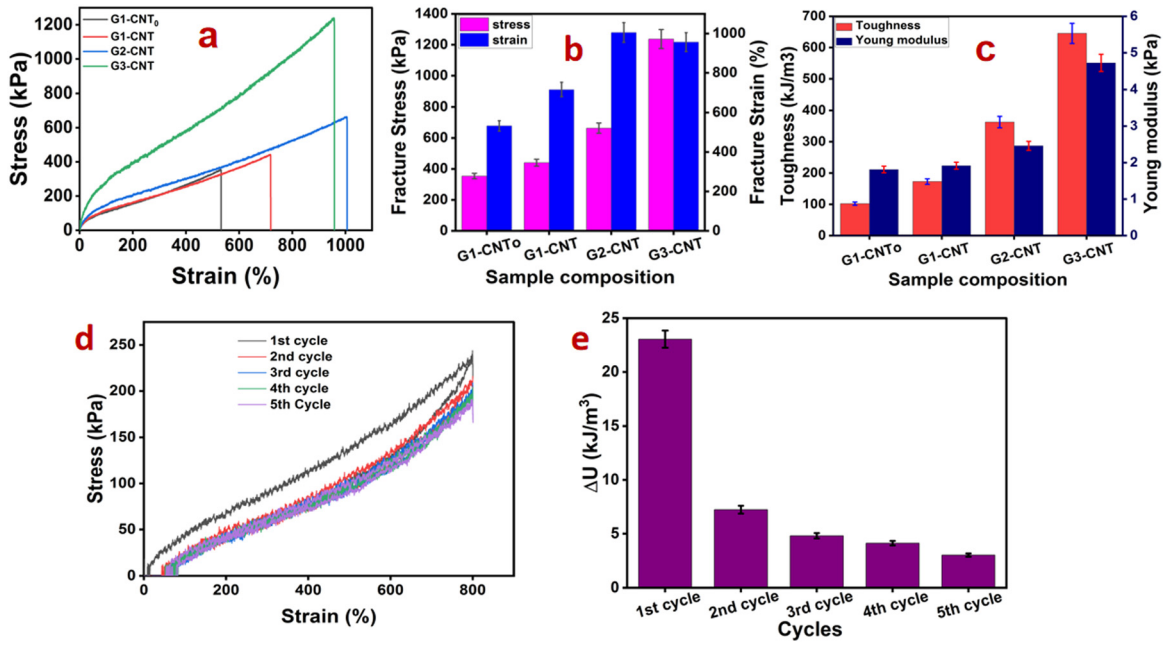

Fig. 2 Mechanical performance of the G3-CNT hydrogel: (a) tensile stress–strain test, (b) fracture stress and strain values, (c) toughness and Young's modulus, (d) cyclic tensile loading–unloading test without any rest time, and (e) dissipated energy in various cycles.

such high stress for the present hydrogel indicates that it is elastically better. However, the value of the dissipation energy decreased to 7.2 kJ m^{-3} (204 kPa), 4.74 kJ m^{-3} (198 kPa), 4.12 kJ m^{-3} (191 kPa), and 3.08 kJ m^{-3} (180 kPa) for the 2nd, 3rd, 4th, and 5th cycle, respectively (Fig. 2e). Such a decrease is the consequence of the breaking of the hydrogel network due to stretching along the applied stress. Hydrogen bonding and hydrophobic association allow the stretching, breaking, and reconstruction of the links. The dissipation energy can be examined for the 1st cycle, which is higher due to the plastic deformation of the materials. However, after the loss of the load, the materials reconstruct the network to its possible limit, showing the rebuilding mechanism of the dynamic bonds of the hydrogel matrix.

3.2 Rheological investigation of G1-CNT_0 and G3-CNT hydrogels

The effect of CNT and different % of GA in hydrogels was elucidated rheologically, and the viscoelastic properties were assessed *via* different tests. An amplitude (strain sweep) test was arranged for the determination of the % strain, linear viscoelastic range (LVR), and the structural strength at 25 °C. The storage (G') and loss (G'') moduli against the % strain were investigated in the range from 0.01% to 1000%. It was observed from Fig. 3a that G' remains higher up to 100%. However, at the critical % strain, the G' decreases while the G'' increases, which suggests that the reverse phenomena of the moduli occurred at the end of LVR. This point of moduli reversal ($G'' > G'$) is the crossing-over point, and a change from the elastic to viscous (liquid-like) behavior of hydrogels takes place. A major observation is the enhancement and shifting of the critical strain from 12.1% for G1-CNT_0 to 56.6% for the G3-CNT sample, which shows the long range LVR of G3-CNT, indicating the increase in % strain and decrease in plastic deformation. Thus, it can be concluded that the materials response is viscoelastic due to the presence of networking within the water medium, and these samples are better candidates for flexible and stretchable

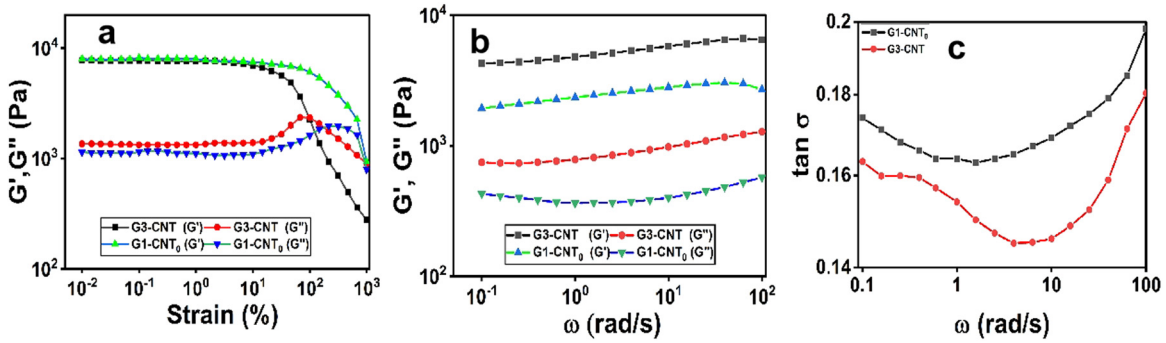

Fig. 3 Rheological investigation of G1-CNT_0 and G3-CNT hydrogels. (a) Strain sweep test, (b) frequency sweep test, and (c) damping factor elucidation.

 © 2025 The Author(s). Published by the Royal Society of Chemistry

Open Access Article. Published on 03 January 2025. Downloaded on 10/26/2025 6:04:59 AM.
This article is licensed under a Creative Commons Attribution-NonCommercial 3.0 Unported Licence.

materials. Another finding was that both G' and G'' moduli of the G3-CNT sample were higher than those of the G1-CNT0 sample, showing the hydrophobic association of the LM monomers within the micelles core of the surfactant, as well as the incorporated CNT. Similarly, in the frequency sweep (FS) shown in Fig. 3b, it can be noted that G' remains higher than G'' for both samples, and almost remains constant at both low and high frequency range. This indicates the material's solid or elastic behavior within the entire range. Furthermore, the higher values of G' and G'' for G3-CNT in comparison to G1-CNT_0 confirm its mechanical and viscoelastic improvement, which is most probably due to the increase in the physical interaction points among the short and long polymer molecules within the hydrogel matrix. The better mechanical property of G3-CNT is also probably due to the proper distribution of CNT within the network, the formation of a proper and balanced microstructure, and the presence of path channels and pores for the mobility of both electrons and ions to achieve good conductivity. The higher value of G' for G3-CNT reflects the effective establishment of the chain network density (CND) with increasing % concentration of GA and CNT addition.[40] Furthermore, the tan δ (damping factor) *vs.* angular frequency was plotted for the demarcation of the viscous and elastic properties of the hydrogels. It is shown in Fig. 3c that both samples show viscoelastic behavior. However, G3-CNT shows a more elastic nature at both lower and high-frequency regions than G1-CNT_0. This is due to the extra crosslinking and interaction within the hydrogel network, which is most probably due to the entanglement of the GA concentration, CNT incorporation, and homogenization.

3.3. Strain sensing behavior

The deformation and current response for strain sensitivity were characterized for strain sensing purposes of the as-synthesized hydrogels. The CNT and NaCl incorporation into the hydrogel enhances the electronic and ion conductivity. The G3-CNT showed a conductivity of 0.142 S m^{-1}, and was used for further strain sensitivity due to its optimized mechanical performance. CNT works both as a physical crosslinker and electronic conducting material, while NaCl shows ionic mobility as Na^+ and Cl^- ions within the gel matrix under the applied potential. The conductivity is associated with the ionic mobility of the ions, as well as the flow of electrons through the pathways and ions channels in the hydrogel network from the developed micropores. The strain sensitivity on the conductive performance was characterized by connecting the hydrogel with two electrodes and LED light. It was found that the light illumination is dependent on the deformation of the hydrogel. A large deformation causes a decrease in brightness and *vice versa* (Fig. 4a and b). Similarly, the hydrogel maintains LED illumination upon complete 360° twisting for a long time (Fig. 4c and d). A load bearing ability of the hydrogel was also checked with a hydrogel strip by hanging a bottle with 2 L of methylene blue solution for a long time (Fig. 4e and f). It was found to be stable and durable without any change.

However, due to the addition of CNT, the decrease in the illumination in G3-CNT is quite small as compared to G1-CNT_0. This is probably due to the CNT homogenization and proper distribution, which provides electronic paths. Meanwhile, upon stretching, the ionic mobility decreases but the electronic communication is still retained up to a greater strain than that of the pure hydrogel having only Na^+ and Cl^- ions. Thus, CNT addition improves both the electrical conductivity and mechanical performance of the as-synthesized hydrogels.

After physical observation, G3-CNT was tested electrochemically by connecting the hydrogel with the electrochemical workstation at an applied potential of 1 V. The sample was stretched at different % strains (50% to 800%), as shown in Fig. 5a. It was

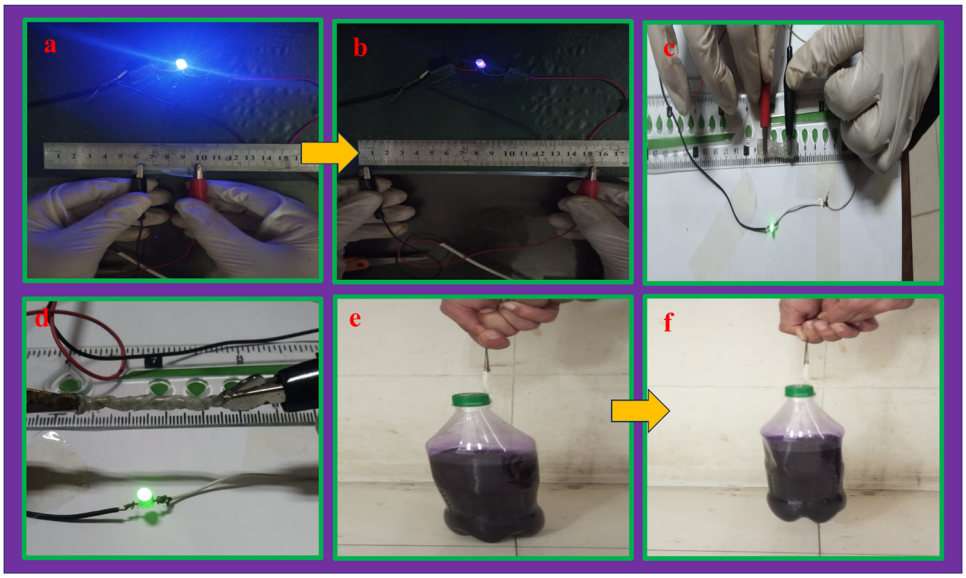

Fig. 4 LED illumination, twisting, and load bearing test for the hydrogel. (a) and (b) LED illumination before and after stretching up to a maximum strain, (c) and (d) twisting, and (e) and (f) load bearing of 2 L methylene blue solution by a hydrogel strip.

Open Access Article. Published on 03 January 2025. Downloaded on 10/26/2025 6:04:59 AM.
This article is licensed under a Creative Commons Attribution-NonCommercial 3.0 Unported Licence.

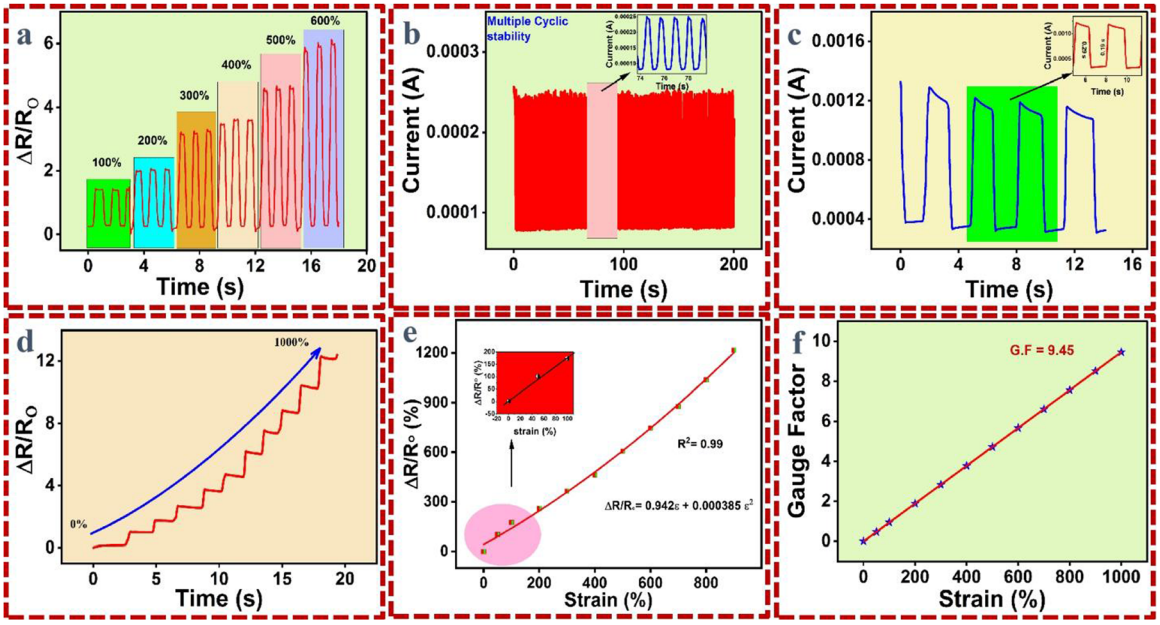

Fig. 5 Strain sensitivity study of G3-CNT. (a) Strain sensitivity (%), (b) multiple cyclic stability, (c) stretching and release response time, (d) relative resistance *vs.* time at different strains (50–1000%), (e) relative resistance (%) with respect to strain (%) and (f) gauge factor (GF) *vs.* strain (%).

noted that the resistance increases due to elongation, which makes it difficult for the ion passage through the pores available for ionic mobility. However, not much reduction was noted due to the presence of electronic mobility, as CNT are homogenized and make serial electrical lines within the hydrogel network. This indicates the materials response even at a higher deformation range. The 200 cyclic stability test was further conducted with the hydrogel for up to 200 s of time. It was found that the cyclic stability is due to the continuous anti-fatigue property of the as-synthesized hydrogel, which in turn is due to the flow of uninterrupted current (Fig. 5b). The hydrogel has been tested by fast and slow chronoamperometry tests to show the sample response under both experimental conditions (Fig. 5c). The sensitivity of the hydrogel was further calculated from the gauge factor (GF) using the previous literature,[41,42] and it was noted to be 9.45 at 1000% strain, as shown in Fig. 5d and f. A straight line is obtained below 100% strain, which shows the application of the as-synthesized hydrogels in the human epidermal skin (Fig. 5e).

3.4. Human motion detection and sensing

The optimized and excellent mechanical properties of the G3-CNT hydrogel sample show its application in sensing. A sample strip was connected to various human body parts, like the finger, wrist, knee, elbow, cheek, *etc.*, and in turn connected with the auto-lab electrochemical station. It was observed that the current drops due to the elongation of the hydrogel on the finger upon bending at one angle in both slow and fast mode (Fig. 6a), as well as at various angles during bending (Fig. 6b). The current response was increased again on the recovery of the hydrogel into its original position when the finger resumed its normal orientation. This restores the pathways for ionic and electronic mobilities. Similarly, the sample was connected to the human elbow, and the response was checked upon bending and relaxation (Fig. 6c). Such responses have applications in the medical field, as well as in robots for their routine work and operation. Pressing the hydrogel materials within the copper mold shows a current response upon pressing the gels between the two soft copper sheets. Two different observations were noted while doing such practical work. When pressing the hydrogel between two copper sheets or writing on the sheet, a response and current were registered. Meanwhile, for writing on the hydrogel surface, the current response dropped (Fig. 6d). Furthermore, the sample was tested mechanically while attached to the human skin of a volunteer. The strain sensing was measured while performing the sit-stand practice (Fig. 6e) and knee bending response (Fig. 6f). The response was almost excellent due to the deformation and relaxation, and the registered current and drops were observed clearly.

Human motion sensing was also characterized further to human voice sensing using the synthesized hydrogel. The sample was connected to the human vocal cord, and different voices expressing the word "school" at low and high pitches were recorded (Fig. 7). The current was dropped due to the stretching and deformation of the vocal cord upon vibration during voice production. This vibration of the vocal cord brings both mechanical strain and sensing to the hydrogel, which is registered in the electrochemical workstation. The relative resistance was measured at both high and low stress. It was found that the hydrogel shows sensing for both high and low stress for the sound "SCHOOL" (Fig. 7a). Similarly, the hydrogel was administered between two copper sheets, and different words like LOVE (Fig. 7b) and TAN (Fig. 7c) were written and different patterns like a leaf (Fig. 7e) and star (Fig. 7f) were drawn. The response was found to be different due to the effect

 © 2025 The Author(s). Published by the Royal Society of Chemistry

Open Access Article. Published on 03 January 2025. Downloaded on 10/26/2025 6:04:59 AM.
This article is licensed under a Creative Commons Attribution-NonCommercial 3.0 Unported Licence.

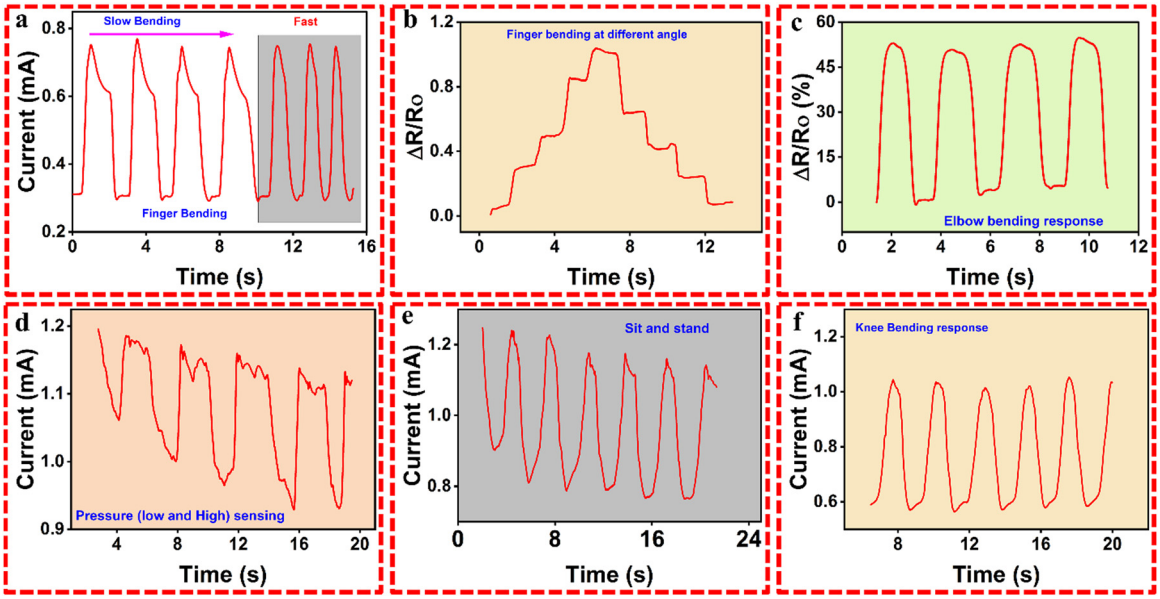

Fig. 6 Human motion detection: (a) slow and fast bending of the finger, (b) finger bending test at different angles, (c) elbow bending response to the volunteer human, (d) pressing the sample at high and low pressure, (e) sit-stand test while attaching the hydrogel to a human knee, and (f) knee bending response of the synthesized sample for sensing purpose.

of the words and writing for each voice, words, and drawing. The G3-CNT hydrogel was further tested by writing directly on the surface of the hydrogel to investigate its sensing for its lowest sensitivity. Different letters like T, A, N, and S, A, N were written on the surface of the hydrogels for observation and examination of the lowest sensitivity level. The hydrogel detected these changes and responded successfully (Fig. 7d), which confirmed the ultra-sensitive nature of these hydrogels.

3.5. Electrochemical performance of G3-CNT for electronic flexible devices

The as-synthesized hydrogels were tested for the electrochemical performance for energy storage devices, like flexible, tractable, and biocompatible supercapacitors. The CV profile of G3-CNT was studied at different scan rates ranging from 10 mV s^{-1} to 100 mV s^{-1}. In the present study, 40 mV s^{-1} was selected for the complete CV blue print analysis. The CV curves shown in

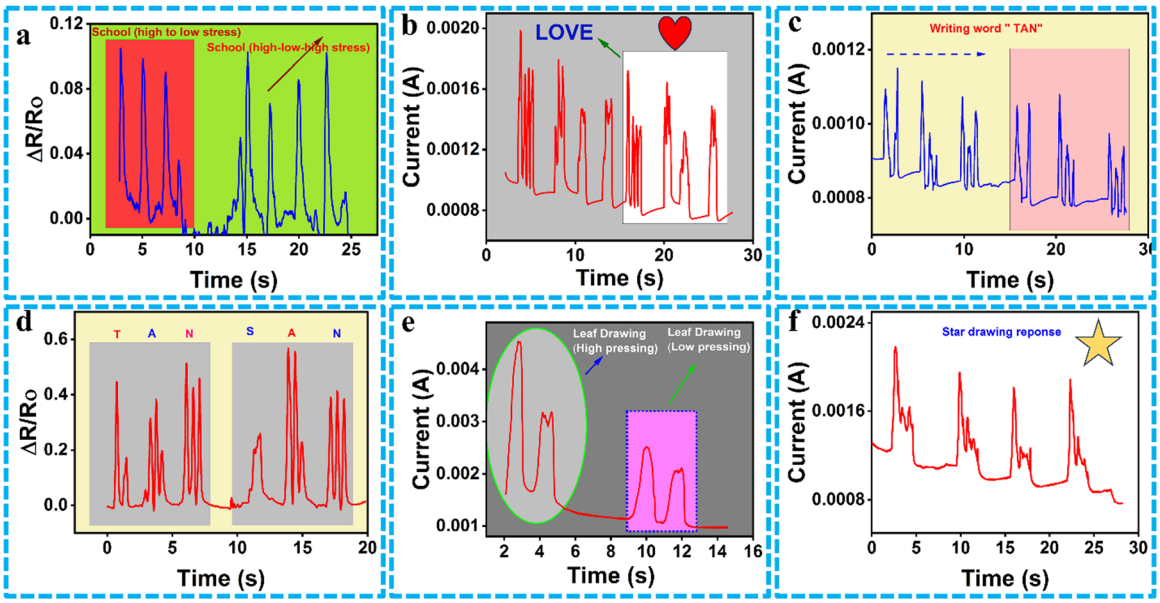

Fig. 7 Hydrogel for human motion detection: (a) voice "school" at low and high stress levels of the vocal cord, (b) writing the word "LOVE" on the hydrogel surface, (c) writing the word "TAN", (d) comparative writing between "TAN" and "SAN", (e) leaf drawing at high and low pressing, and (f) drawing "star" on a hydrogel.

Open Access Article. Published on 03 January 2025. Downloaded on 10/26/2025 6:04:59 AM.
This article is licensed under a Creative Commons Attribution-NonCommercial 3.0 Unported Licence.

Fig. 8a exhibit a rectangular symmetrical characteristic shape of the almost electric-double-layer capacitor (EDLC) behavior. The area under the enclosed curve indicated the specific capacitance (Cs) with the highest value for the sample G3-CNT at a scan rate of 20 mV s^{-1}. The Cs value was calculated from the CV loop area of the curve, as well as the weight of the material with the help of the equation, $Cs = A/m \times \Delta V \times k$, where A is the area of the polygon (integrated), m is the mass taken of the material, ΔV is a potential window (V), and k is the scan rate (mV s^{-1}). The Cs for G3-CNT were found to be 166.6, 171.25, 166.6, 158.3, 152.08, and 146.6 F g^{-1} at scan rates of 10, 20, 40, 60, 80, and 100 mV s^{-1}, respectively. It can be noted from Fig. 8b that the Cs increase from 100 mV s^{-1} up to 20 mV s^{-1}, and then decrease at the low scan rates of 10 and 5 mV s^{-1}. This is due to the internal high resistance of the material to the low scan rate. The Cs decrease is also due to the lack of proper timing for electrolyte involvement in the electrochemical reaction. The highest Cs was found at 20 mV s^{-1} (171.25 F g^{-1}) in the present study. This is most probably due to the proper timing for the electrolytes to be involved in the electrochemical process, as well as the material internal resistance balance to the mentioned scan rate. It should be noted that the rectangular voltammogram retains its shape even at a higher scan rate, indicating the better performance of the G3-CNT hydrogel.

The galvanostatic charge–discharge GCD study shows almost triangular symmetrical curves for the G3-CNT hydrogel (Fig. 8c). The Cs have been calculated *via* equation $Cs = I \times \Delta t/\Delta V \times m$, where Δt is the discharge timing and I/m is the current density (A g^{-1}) applied. The Cs found for G3-CNT are 113.7, 89.1, 60.75, 37.5, and 18.75 F g^{-1} at 0.3, 0.7, 0.9, 1.0, and 1.5 A g^{-1} current density, respectively. Furthermore, the electrochemical response of the G3-CNT electrode in the three-electrode system as a working electrode showed better capacitive performance during the GCD test. This is because there was a small drop in the internal resistance (IR) in the charging–discharging process, as shown in Fig. 8c. Such performance is necessary for electrode materials in energy storage devices with little or very minute energy dissipation. Thus, it can be established from the finding that the CNT are stabilized and homogenized in the stabilizing and reinforcing agent, GA, within the hydrogel network materials with improved electrochemical and conducive properties. The better Cs performance of the G3-CNT sample is due to the homogeneous and complete dispersion of

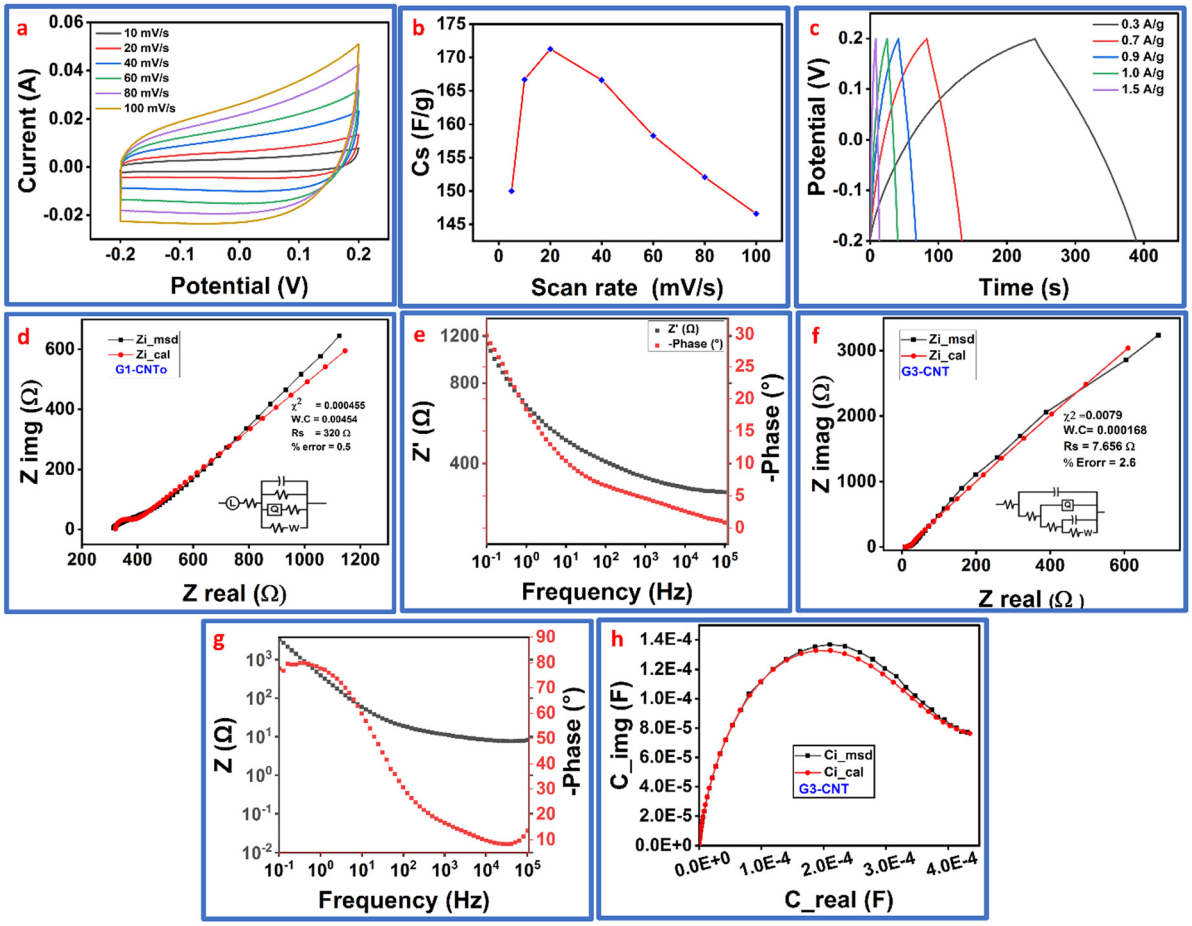

Fig. 8 Electrochemical properties; (a) CV at different scan rates for G3-CNT, (b) specific capacitance (F g^{-1}) *vs.* different scan rates for G3-CNT, (c) GCD at different current densities for G3-CNT, (d) EIS Nyquist for G1-CNT_0, (e) Bode plot of G1-CNT_0, (f) Nyquist plot of G3-CNT and electronic circuit inset, (g) G3-CNT bode plot at high and low frequency regions, and (h) G3-CNT capacitance between imaginary and real values.

 © 2025 The Author(s). Published by the Royal Society of Chemistry

Open Access Article. Published on 03 January 2025. Downloaded on 10/26/2025 6:04:59 AM.
This article is licensed under a Creative Commons Attribution-NonCommercial 3.0 Unported Licence.

Table 1 Performance comparison of the flexible and stretchable strain sensors and supercapacitors with those reported in previous studies

Hydrogels	Current density	Specific capacitance	Gauge factor (GF)	Ref.
rMGO-GG/PVA-b	0.3 A g^{-1}	108.33 F g^{-1}	8.25	17
(PAM)/PDA conductive hydrogels @ DES (HDES/CCNF)	1 mA cm^{-2}	108.37 mF cm^{-2}	1.17	43
CPF4 films @ filter paper/PVA/H_2SO_4	0.4 mA cm^{-2}	111 mF cm^{-2}	Nil	44
H-Gel/AS-MWCNTs-PPy-AS	0.5 A g^{-1}	112 F g^{-1}	6.8	45
(TC-*s*-CNT-PS)	0.5 A g^{-1}	65 F g^{-1}	Nil	46
agar/PAA-Al^{3+} DES gels	0.8 A g^{-1}	66.7 F g^{-1}	1.21	47
G3-CNT hydrogels	0.3 A g^{-1}	113.7 F g^{-1}	9.45	Present work

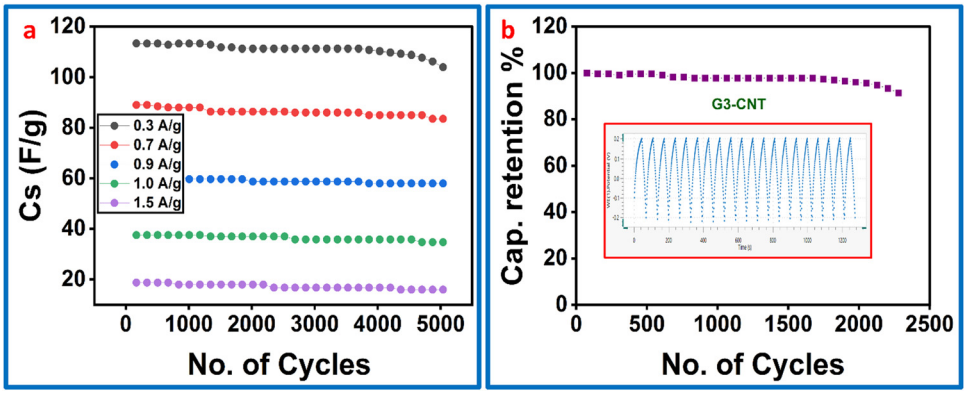

Fig. 9 Performance evaluation of the G3-CNT hydrogel; (a) Cs (F g^{-1}) after 5000-cycle operation and (b) capacitance retention % *vs.* number of cycles.

CNT at higher concentrations of GA, thus developing micro-channel pathways for the electronic and ionic conductivity, and making the hydrogel a better electrode for energy storage devices like supercapacitors.

Electrochemical impedance spectroscopy (EIS) was further performed with the G1-CNT_0 and G3-CNT hydrogels at 5 mV to avoid destroying the samples. Different plots, including Nyquist, Bode, and capacitance, were obtained. A semi-circle observed in Fig. 8(d and f) indicated the transfer of electrons mechanism between the electrodes in a three-electrode or 2 electrode system, and indicated the IR of the electrolytes of the materials. Meanwhile, at lower frequency, a long straight line was observed (Warburg (*W*)), which is the impedance constant and exhibits the active materials used as an electrode for the diffusion of charge. All these characteristics show the excellent performance of the synthesized hydrogels. From the intercept of the horizontal axis of the small semi-circle, the IR values were calculated and found to be 7.656 Ω and 320 Ω for the G3-CNT and G1-CNT_0 hydrogels, respectively, in the high frequency (*f*) range. Similarly, both calculated and measured values are fitted *via* NOVA, and the electronic circuits for both samples are shown in the Nyquist, Bode, and capacitance plots (Fig. 8d–h). Table 1 presents the key performance parameters of the current work.

The multicycle performance of the electrode G3-CNT was also evaluated regarding its Cs, as well as capacitance retention %, as shown in Fig. 9a and b. The performance evaluation of G3-CNT for electrode purposes in the application within flexible soft energy storage devices revealed its excellent stability during routine operation. The Cs (F g^{-1}) at different current densities ranging from 0.3 to 1.5 A g^{-1} were studied, and there was little fluctuation in the Cs value after 5000 cycles (Fig. 9a). Similarly, the capacitance retention % was sustained up to 91% after 2500 cycles of operation (Fig. 9b). These results are due to the better homogenization of CNT *via* stabilizer and reinforcement of GA to build the microstructure of the improved and enhanced 3D hydrogel network, which in turn provides mechanical support, conductivity, and proper pathway channels for transport of both ions and electrons within the electrode materials. The higher GA concentration not only improves the mechanical performance, but also helps to avoid the CNT agglomeration. Due to the hydrophobic nature and association of CNT, this results in π–π interactions of strong van der Waals forces and agglomeration, which in turn negatively affects the cross-linking and electrical performance of the hydrogel. However, in the present case, such better performance is due to the better configurational hydrogel structure, which not only gives stability but also enhances the mechanical behavior after thousands of cycles of operation in the electrochemical process.

4. Conclusion

The two-fold application of the present CNT-based synthesized hydrogels indicate the applicability in human motion detection with better sensitivity at different % strain, and the electrochemical performance as an electrode material for flexible soft electronic energy storage devices. It was rheologically found that hydrogels have better viscoelastic performance in the LVR range regarding the critical strain. The mechanical properties

Open Access Article. Published on 03 January 2025. Downloaded on 10/26/2025 6:04:59 AM.
This article is licensed under a Creative Commons Attribution-NonCommercial 3.0 Unported Licence.

of stretchability, toughness, energy dissipation, and antifatigue were found to be better. The conductivity of the hydrogel materials was calculated to be 0.142 S m^{-1} for the strain sensing of the materials. The electrochemical properties were evaluated, revealing a specific capacitance (Cs) of 171.25 F g^{-1} from CV measurements at a scan rate of 20 mV s^{-1}, and 113.7 F g^{-1} from GCD measurements at a current density of 0.3 A g^{-1}. From the EIS study, the resistance of the present CNT-based biopolymeric hydrogel was found to be 7.65 Ω, which also supports low-resistance materials, and is applicable in the designing of electrode materials in soft flexible energy storage devices like supercapacitors.

Data availability

This work is original research, with primary research/new data available in figures.

Conflicts of interest

The authors declare that there are no conflicts of interest.

References

1 Z. Wang, Y. Cong and J. Fu, Stretchable and tough conductive hydrogels for flexible pressure and strain sensors, *J. Mater. Chem. B*, 2020, **8**(16), 3437–3459.
2 X. Liu, *et al.*, Biomimetic integration of tough polymer elastomer with conductive hydrogel for highly stretchable, flexible electronic, *Nano Energy*, 2022, **92**, 106735.
3 W. Dai, *et al.*, Highly stretchable, ultra-sensitive, and self-healable multifunctional flexible conductive hydrogel sensor for motion detection and information transmission, *ACS Appl. Mater. Interfaces*, 2023, **15**(24), 29499–29510.
4 M. Khan, *et al.*, Multi-role conductive hydrogels for flexible transducers regulated by MOFs for monitoring human activities and electronic skin functions, *J. Mater. Chem. B*, 2024, **12**, 6190–6202.
5 K. Chen, *et al.*, Ultra-stretchable, adhesive, and self-healing MXene/polyampholytes hydrogel as flexible and wearable epidermal sensors, *Colloids Surf., A*, 2022, **645**, 128897.
6 M. Khan, *et al.*, Bimetallic-MOF Tunable Conductive Hydrogels to Unleash High Stretchability and Sensitivity for Highly Responsive Flexible Sensors and Artificial Skin Applications, *ACS Appl. Polym. Mater.*, 2024, **6**(12), 7288–7300.
7 S. Xia, *et al.*, A flexible, adhesive and self-healable hydrogel-based wearable strain sensor for human motion and physiological signal monitoring, *J. Mater. Chem. B*, 2019, **7**(30), 4638–4648.
8 L. Dong, *et al.*, Stretchable, adhesive, self-healable, and conductive hydrogel-based deformable triboelectric nanogenerator for energy harvesting and human motion sensing, *ACS Appl. Mater. Interfaces*, 2022, **14**(7), 9126–9137.
9 X. Di, *et al.*, A bio-inspired, ultra-tough, high-sensitivity, and anti-swelling conductive hydrogel strain sensor for motion detection and information transmission, *Mater. Horiz.*, 2022, **9**(12), 3057–3069.
10 M. Zheng, *et al.*, Skin-inspired gelatin-based flexible bioelectronic hydrogel for wound healing promotion and motion sensing, *Biomaterials*, 2021, **276**, 121026.
11 V. R. Feig, *et al.*, Mechanically tunable conductive interpenetrating network hydrogels that mimic the elastic moduli of biological tissue, *Nat. Commun.*, 2018, **9**(1), 2740.
12 R. Ullah, *et al.*, The development of anti-freezing and anti-evaporating conductive organohydrogel for flexible strain-sensing electronic devices, *RSC Adv.*, 2024, **14**(42), 30886–30895.
13 B. Guo, *et al.*, Properties of conductive polymer hydrogels and their application in sensors, *J. Polym. Sci., Part B: Polym. Phys.*, 2019, **57**(23), 1606–1621.
14 C. Xiong, *et al.*, Electroactive biopolymer/graphene hydrogels prepared for high-performance supercapacitor electrodes, *Electrochim. Acta*, 2016, **211**, 941–949.
15 A. Xavier Mendes, *et al.*, Enhanced electroactivity, mechanical properties, and printability through the addition of graphene oxide to photo-cross-linkable gelatin methacryloyl hydrogel, *ACS Biomater. Sci. Eng.*, 2021, **7**(6), 2279–2295.
16 J. L. Aparicio-Collado, *et al.*, Electroactive calcium-alginate/polycaprolactone/reduced graphene oxide nanohybrid hydrogels for skeletal muscle tissue engineering, *Colloids Surf., B*, 2022, **214**, 112455.
17 T. Ur Rehman, L. A. Shah and M. Khan, Multifunctional and self-healable conductive IPN hydrogels functionalized with reduced magnetite graphene oxide for an advanced flexible all in one solid-state supercapacitor, *Mater. Adv.*, 2024, **5**(2), 806–819.
18 Z. Ying, *et al.*, Novel electrically-conductive electro-responsive hydrogels for smart actuators with a carbon-nanotube-enriched three-dimensional conductive network and a physical-phase-type three-dimensional interpenetrating network, *J. Mater. Chem. C*, 2020, **8**(12), 4192–4205.
19 S. Liu, *et al.*, Highly Stretchable and Self-Healing Strain Sensor Based on Gellan Gum Hybrid Hydrogel for Human Motion Monitoring, *ACS Appl. Polym. Mater.*, 2020, **2**(3), 1325–1334.
20 T. Zhu, *et al.*, Recent advances in conductive hydrogels: classifications, properties, and applications, *Chem. Soc. Rev.*, 2023, **52**(2), 473–509.
21 Y. Zhao, *et al.*, Microgel-enhanced double network hydrogel electrode with high conductivity and stability for intrinsically stretchable and flexible all-gel-state supercapacitor, *ACS Appl. Mater. Interfaces*, 2018, **10**(23), 19323–19330.
22 F. Ding, *et al.*, Self-healing and tough hydrogels with conductive properties prepared through an interpenetrating polymer network strategy, *Polymer*, 2020, **206**, 122907.
23 A. Wang, *et al.*, Hydrogen-bonded network enables semi-interpenetrating ionic conductive hydrogels with high stretchability and excellent fatigue resistance for capacitive/resistive bimodal sensors, *Chem. Eng. J.*, 2021, **411**, 128506.
24 D. Liu, *et al.*, Conductive polymer based hydrogels and their application in wearable sensors: a review, *Mater. Horiz.*, 2023, **10**(8), 2800–2823.

 © 2025 The Author(s). Published by the Royal Society of Chemistry

Open Access Article. Published on 03 January 2025. Downloaded on 10/26/2025 6:04:59 AM.
This article is licensed under a Creative Commons Attribution-NonCommercial 3.0 Unported Licence.

25 X. Wang, *et al.*, Stretch-induced Conductivity Enhancement in Highly Conductive and Tough Hydrogels, *Adv. Mater.*, 2024, 2313845.
26 M. Sher, *et al.*, Facile fabrication of stretchable, anti-freezing, and stable organohydrogels for strain sensing at subzero temperatures, *Mater. Adv.*, 2024, **5**(20), 8164–8176.
27 W. Deng, F. Wei and J. Hu, Muscle contraction-inspired tough hydrogels, *ACS Appl. Mater. Interfaces*, 2023, **15**(6), 8462–8470.
28 L. Yang, *et al.*, Ultra-stiff and tough hydrogels based on small but strong hydrophobic associations via a low-reactive hydrophilic monomer, *Polym. Chem.*, 2023, **14**(18), 2212–2219.
29 Y. Xie, *et al.*, Carbon Nanotubes and Silica@ polyaniline Core–Shell Particles Synergistically Enhance the Toughness and Electrical Conductivity in Hydrophobic Associated Hydrogels, *Langmuir*, 2023, **39**(3), 1299–1308.
30 M. Khan, *et al.*, Cellulose nanocrystals boosted hydrophobic association in dual network polymer hydrogels as advanced flexible strain sensor for human motion detection, *J. Mech. Behav. Biomed. Mater.*, 2023, **138**, 105610.
31 Y. Xin, *et al.*, Tough, healable, and sensitive strain sensor based on multiphysically cross-linked hydrogel for ionic skin, *Biomacromolecules*, 2023, **24**(3), 1287–1298.
32 B. Xue, *et al.*, Strong, tough, rapid-recovery, and fatigue-resistant hydrogels made of picot peptide fibres, *Nat. Commun.*, 2023, **14**(1), 2583.
33 M. Khan, *et al.*, Multiple-Language-Responsive Conductive Hydrogel Composites for Flexible Strain and Epidermis Sensors, *ACS Appl. Polym. Mater.*, 2024, **6**(7), 4233–4243.
34 K. Sharma, *et al.*, Gum ghatti based novel electrically conductive biomaterials: A study of conductivity and surface morphology, *eXPRESS Polym. Lett.*, 2014, **8**, 4.
35 J.-L. Xu and A. A. Gowen, Time series Fourier transform infrared spectroscopy for characterization of water vapor sorption in hydrophilic and hydrophobic polymeric films, *Spectrochim. Acta, Part A*, 2021, **250**, 119371.
36 M. S. Deshpande and S. Mazumdar, Sequence specific association of tryptic peptides with multiwalled carbon nanotubes: effect of localization of hydrophobic residues, *Biomacromolecules*, 2012, **13**(5), 1410–1419.
37 B. P. Singh, *et al.*, Solvent Free, Efficient, Industrially Viable, Fast Dispersion Process Based Amine Modified MWCNT Reinforced Epoxy Composites Of Superior Mechanical Properties, *Adv. Mater. Lett.*, 2015, **6**, 104–113.
38 I. T. Rakipov, *et al.*, FTIR spectral study of intermolecular interactions of C= O groups of amides in solution, *J. Mol. Liq.*, 2022, **354**, 118838.
39 R. Zhao, *et al.*, Multifunctional Conductive Double-Network Hydrogel Sensors for Multiscale Motion Detection and Temperature Monitoring, *ACS Appl. Mater. Interfaces*, 2023, **15**(51), 59854–59865.
40 M. Sun, *et al.*, Multi-sacrificial bonds enhanced double network hydrogel with high toughness, resilience, damping, and notch-insensitivity, *Polymers*, 2020, **12**(10), 2263.
41 M. Khan, *et al.*, Flexible Ionic Conductive Hydrogels with Wrinkled Texture for Flexible Strain Transducer with Language Identifying Diversity, *Chem. Mater.*, 2024, **36**(9), 4703–4713.
42 R. Ullah, L. A. Shah and M. T. Khan, Cellulose nanocrystals boosted hydrophobically associated self-healable conductive hydrogels for the application of strain sensors and electronic devices, *Int. J. Biol. Macromol.*, 2024, **260**, 129376.
43 Q. Li, *et al.*, Multifunctional conductive hydrogels for wearable sensors and supercapacitors, *J. Mater. Chem. A*, 2024, **12**(6), 3589–3600.
44 M. P. Sidheekha, *et al.*, Conducting polymer/hydrogel hybrid free-standing electrodes for flexible supercapacitors capable of self-sensing working conditions: large-scale fabrication through facile and low-cost route, *Eng. Sci.*, 2023, **23**(7), 890.
45 C. Liu, *et al.*, Self-healable, high-strength hydrogel electrode for flexible sensors and supercapacitors, *ACS Appl. Mater. Interfaces*, 2021, **13**(30), 36240–36252.
46 Y. Wu, *et al.*, Using TEMPO-oxidized-nanocellulose stabilized carbon nanotubes to make pigskin hydrogel conductive as flexible sensor and supercapacitor electrode: Inspired from a Chinese cuisine, *Compos. Sci. Technol.*, 2020, **196**, 108226.
47 L. Wu, *et al.*, Highly Stretchable, self-recoverable, and conductive double-network gels containing deep eutectic solvent for a flexible supercapacitor and strain sensor, *J. Electron. Mater.*, 2022, **51**(9), 5074–5086.